Chemical Science

ROYAL SOCIETY OF CHEMISTRY

EDGE ARTICLE

View Article Online
View Journal | View Issue

Cite this: *Chem. Sci.*, 2022, **13**, 11083

All publication charges for this article have been paid for by the Royal Society of Chemistry

Received 12th July 2022
Accepted 18th August 2022

DOI: 10.1039/d2sc03885d

rsc.li/chemical-science

Surface differences of oxide nanocrystals determined by geometry and exogenously coordinated water molecules†

Junchao Chen,‡[ab] Xin-Ping Wu,‡[c] Michael A. Hope,‡[d] Zhiye Lin,[a] Lei Zhu,[e] Yujie Wen,[a] Yixiao Zhang,[b] Tian Qin,[b] Jia Wang,[c] Tao Liu,[f] Xifeng Xia,[g] Di Wu,[h] Xue-Qing Gong,[c] Weiping Tang,[e] Weiping Ding,[a] Xi Liu,[b] Liwei Chen,[bi] Clare P. Grey[d] and Luming Peng*[ajk]

Determining the different surfaces of oxide nanocrystals is key in developing structure–property relations. In many cases, only surface geometry is considered while ignoring the influence of surroundings, such as ubiquitous water on the surface. Here we apply ^{17}O solid-state NMR spectroscopy to explore the facet differences of morphology-controlled ceria nanocrystals considering both geometry and water adsorption. Tri-coordinated oxygen ions at the 1st layer of ceria (111), (110), and (100) facets exhibit distinct ^{17}O NMR shifts at dry surfaces while these ^{17}O NMR parameters vary in the presence of water, indicating its non-negligible effects on the oxide surface. Thus, the interaction between water and oxide surfaces and its impact on the chemical environment should be considered in future studies, and solid-state NMR spectroscopy is a sensitive approach for obtaining such information. The work provides new insights into elucidating the surface chemistry of oxide nanomaterials.

Introduction

Different surfaces of oxides[1,2] usually exhibit diverse properties in heterogeneous catalysis,[3–5] photocatalysis,[6–8] gas sensors,[9] energy storage,[10] and biological applications.[11] Identification of the chemical environment of different surfaces is, therefore a prerequisite for investigating structure–property relations for oxides. The most popular conventional techniques for determining surface geometry are microscopy-based methods, including Scanning Electron Microscopy (SEM),[12,13] High-Resolution Transmission Electron Microscopy (HRTEM)[14,15] and Scanning Tunneling Microscopy (STM),[16,17] with which the surfaces can be visualized at controlled temperature and pressure conditions, and even in gas or liquid environments with specialized setups.[14,16] However, disadvantages remain in the application of such techniques, due to the weak signatures of light elements (*e.g.*, H and O) for oxide and oxide-based materials.[18] Complementary spectroscopy-based techniques, such as infrared[19,20] and solid-state nuclear magnetic resonance (NMR) spectroscopy,[21–23] have been applied to overcome these problems, however, the use of probe molecules (*e.g.*, CO and trimethylphosphine) is often required. In addition to the geometry information obtained from these methods, the chemical environment which may also include the influence of surroundings, is still challenging to probe. For instance, water is ubiquitous in nature and is often involved in surface processes,[24,25] yet the impact of water on oxide surfaces[26,27] is still not well studied.

[a]*Key Laboratory of Mesoscopic Chemistry of MOE, Collaborative Innovation Center of Chemistry for Life Sciences, School of Chemistry and Chemical Engineering, Nanjing University, 163 Xianlin Road, Nanjing 210023, China. E-mail: luming@nju.edu.cn*

[b]*School of Chemistry and Chemical Engineering, Frontiers Science Center for Transformative Molecules, In situ Center for Physical Sciences, Shanghai Jiao Tong University, Shanghai 200240, China*

[c]*Key Laboratory for Advanced Materials, Centre for Computational Chemistry, Research Institute of Industrial Catalysis, East China University of Science and Technology, 130 Meilong Road, Shanghai 200237, China*

[d]*Department of Chemistry, University of Cambridge, Lensfield Road, Cambridge CB2 1EW, UK*

[e]*State Key Laboratory of Space Power Technology, Shanghai Institute of Space Power-Sources (SISP), Shanghai Academy of Spaceflight Technology, Shanghai 200245, China*

[f]*Shanghai Key Laboratory of Chemical Assessment and Sustainability, Department of Chemistry, Tongji University, Shanghai 200092, China*

[g]*Analysis and Testing Center, Nanjing University of Science and Technology, Nanjing 210094, China*

[h]*College of Food Science and Engineering/Collaborative Innovation Center for Modern Grain Circulation and Safety/Key Laboratory of Grains and Oils Quality Control and Processing, Nanjing University of Finance and Economics, Nanjing 210023, China*

[i]*i-Lab, CAS Center for Excellence in Nanoscience, Suzhou Institute of Nano-Tech and Nano-Bionics (SINANO), Chinese Academy of Sciences, Suzhou 215123, China*

[j]*Jiangsu Key Laboratory of Vehicle Emissions Control, Nanjing University, Nanjing 210093, China*

[k]*Frontiers Science Center for Critical Earth Material Cycling (FSC-CEMaC), Nanjing University, Nanjing, Jiangsu, 210023, China*

† Electronic supplementary information (ESI) available. See https://doi.org/10.1039/d2sc03885d

‡ These authors contributed equally.

Recently, we showed that ^{17}O solid-state NMR in combination with ^{17}O surface-selective labeling and density functional theory (DFT) calculations can probe the oxygen anions of oxide surfaces with a very high sensitivity.[18,28–30] In particular, we have applied this strategy to study the dominant surfaces of some morphology-controlled ceria nanostructures, which are technologically important in CO oxidation,[31] automotive three-way catalysis[32] and the water–gas shift (WGS) reaction.[33] We found that the 1st, 2nd and 3rd layer oxygen ions as well as surface hydroxyl groups at ceria (111) surface can be distinguished,[29] while the reconstruction of ceria (100) surfaces[18] and the hydrous ceria (111) surfaces can be elucidated.[30] Here we adopt a strategy based on ^{17}O NMR spectroscopy combined with an improved^{17}O surface-selective labelling method (increased rounds of labelling that for the first time, enables us to probe not only the dominant surfaces but also secondary exposed ones) to ceria nanorods containing mixed facets, and reveal the differences of ceria (111), (110) and (100) surfaces under dry and hydrated conditions. We found both the surface geometry and exogenously coordinated water molecules are non-ignorable for determining the chemical environment of oxide surfaces.

Results and discussion

Morphology of the ceria nanorods

Faceted ceria nanorods were synthesized *via* a solvothermal approach.[34] Two samples were prepared with different annealing temperatures (see Methods): NRs700 (nanorods annealed at 700 °C) and NRs300 (nanorods annealed at 300 °C). Scanning transmission electron microscopy (STEM) and HRTEM images in Fig. 1 depict the exposed surfaces of NRs700 and NRs300. Fig. 1a and c exhibit several nanorods measuring around 15–20 nm in width, for NRs700 and NRs300, respectively. Fig. 1b shows that NRs700 is mainly dominated by (111) surfaces along the sides of the nanorods, with a small fraction of (110) and (100) secondary surfaces at the ends. Two images of NRs300 are presented in Fig. 1d and e along with the corresponding Fourier transform (FT) patterns. The strongest electron diffraction peaks in Fig. 1d are assigned to the (111) and (100) peaks, while those in Fig. 1e only correspond to the (100) peak, suggesting the NRs300 predominantly expose (110) and (100) surfaces. All the microscopy signatures are consistent with previous results by Gao *et al.*[34] Synchrotron powder X-ray diffraction (XRD) (Fig. S1†) confirms that both samples crystallize with the fluorite structure (space group: $Fm\bar{3}m$); the broad diffraction peaks denote that they are nano-sized crystals. The BET surface areas of NRs700 and NRs300 (Fig. S2 and Table S1†) are determined as 110.9 and 132.7 $m^2\ g^{-1}$, respectively. Na^+ or NO_3^- impurities from the NaOH and $Ce(NO_3)_3\cdot 6H_2O$ precursors are not detectable by X-ray photoelectron spectra (XPS) (Fig. S3†), inductively coupled plasma mass spectrometry (ICP-MS) or elemental analysis (Table S1†); therefore, possible surface impurities are not considered.

Conventional ^{17}O NMR spectroscopy

Following four rounds of isotopic labeling with 90 atom% $^{17}O_2$, resulting in a surface with highly enriched oxygen ions at the 1st and 2nd layers (see Methods), the NRs700 and NRs300 were subjected to ^{17}O solid-state NMR measurements. Since dry $^{17}O_2$ was used in the enrichment, the samples should represent dry surfaces (*vide infra*). The most intense resonance at 877 ppm in the ^{17}O NMR spectra of both samples (Fig. 2a and the untruncated spectra in Fig. S4†) arises from the tetra-coordinated oxygen ion (O_{4C}) in the bulk.[29] The signal at a higher frequency of 1032 ppm for NRs700 is due to tri-coordinated oxygen ions (O_{3C}) at the first layer of the major (111) facet, while the relatively sharp signal at 970 ppm in both samples comes from O_{3C}s at the 1st layer of ceria (100) surfaces (Fig. 2b).[18,30] The broader signal at ~1020 ppm for both samples, which has not previously been assigned, may be tentatively attributed to the oxygen ions at the 1st layer of other low-index ceria surfaces, most likely the (110) surface given that there is a significant proportion of (110) facets in the NRs300 sample. Other ^{17}O resonances at 920, 905 and 830 ppm are associated with O_{4C}s at the sub-surface layers of (111) and (100) facets.[18,30] Notably, the ^{17}O NMR signals of the 1st layer O_{3C}s for different dry ceria surfaces are distinct, proving that the chemical environment of the exposed low-coordinated oxygen ions depends critically on the surface geometry.

Recent investigations have shown that a fraction of dry ceria (110) surfaces, which have a relatively high surface energy (1.00 J m^{-2}), can reconstruct to yield indent (111) nanofacets with a lower surface energy (0.88 J m^{-2}).[19,35] To investigate the presence of (111) nanofacets at the (110) surfaces of the nanorod samples, DFT simulations were conducted on two models with and without reconstruction (Fig. 2b, S5–S9, Tables S2 and S3†). For the dry (110) surface, a single shift (δ_{CG}) of 1052 ppm for 1st layer O_{3C} is predicted (Table S2 and Fig. S9†); although a non-zero ^{17}O spectral intensity is observed at this frequency, the dry (110) surface alone is not sufficient to explain the broad resonance centered at ~1020 ppm. Including the reconstructed (110) surface yields further O_{3C} δ_{CG}s at 1033 and 1008 ppm (Fig. S9† and 3a), explaining the broad experimental signal, especially considering that the presence of any surface defects and/or vacancies will cause further broadening.[29] This provides further experimental evidence for the reconstruction of the (110) surface. In addition, the absence of signal at 920 ppm in both the experimental spectrum of NRs300 (Fig. 2) and the simulated spectrum based on DFT calculations (Fig. S9†) shows that the (111) nanofacets reconstructed from (110) facets can be distinguished from the common (111) surfaces. The simulated δ_{CG}s for O_{4C}s in the sub-surface layers and the bulk of both models are between 898 and 800 ppm, in accordance with the remaining intensity observed in this region (Fig. 2).

^{17}O DNP NMR spectroscopy

Direct dynamic nuclear polarization (DNP) is another advanced approach to selectively observe the surface ^{17}O NMR signals of oxides.[36–39] The sample is wetted with a solution of organic radicals, cooled to 100 K, and irradiated with microwaves in order to transfer polarization from the unpaired electrons and enhance the ^{17}O NMR signals of oxygen ions at or near the surface. The direct DNP ^{17}O NMR spectra of $^{17}O_2$-labeled

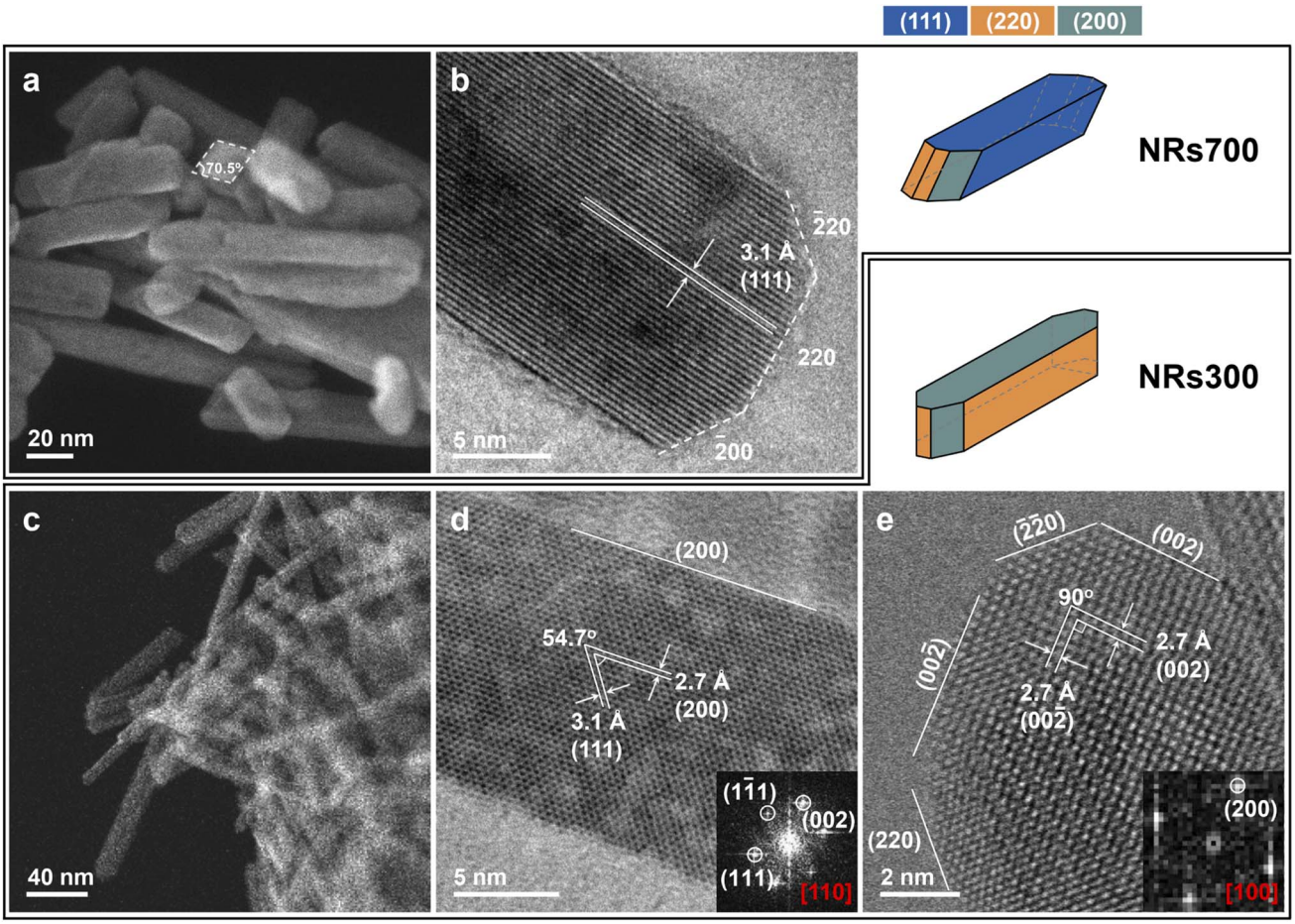

Fig. 1 STEM images and morphology models (top right corner) of NRs700 and NRs300. (a) Secondary electron (SE) and (b) HRTEM images of NRs700. (c) SE and (d and e) HRTEM images of NRs300 (the insets show the corresponding FT patterns that allow assignment of the planes perpendicular to the observation axes of (d) [110] and (e) [100], respectively).

NRs700 and NRs300 (Fig. S10†) exhibit an order-of-magnitude signal enhancement and similar signals to the conventional spectra of surface-selectively labelled samples, but suffer from poor resolution due to increased signal broadening at 100 K and the overlap of spinning sidebands at the higher field and lower magic angle spinning (MAS) rate. On the other hand, the conventional ^{17}O NMR spectra of surface-selectively enriched ceria nanocrystals show much improved resolution with relatively good signal-to-noise ratios, which should represent a better approach for obtaining surface structural information. These results are in agreement with our previous studies on the optimal strategy for surface investigations.[30]

Spectral assignments from DFT calculations

Compared to ^{17}O-enrichment with $^{17}O_2$ gas, enrichment with $H_2{}^{17}O$ is more surface-selective and results in highly hydrated surfaces.[29,30] The ^{17}O NMR spectra of ceria NRs700 and NRs300 enriched with $H_2{}^{17}O$ were therefore recorded to study the structure of hydrous ceria surfaces (Fig. 3a). The resonance at 877 ppm arising from bulk O_{4C}s exhibits a low intensity in both spectra, indicating a low degree of labeling for bulk oxygen ions. Other resonances exhibit notable distinctions from those in Fig. 2a. The major signal for NRs700 occurs at 894 ppm, which is due to the 1st and 2nd layer oxygen ions of hydrated ceria (111) surfaces, as previously determined from DFT calculations (Fig. 3b).[30] Another previously unobserved resonance at 862 ppm is ascribed to the 3rd layer O_{4C}s in hydrated (111) surfaces on the basis of DFT calculations, which may not have been effectively labelled with shorter thermal treatment times in the previous study.[30] The broad peak at ~1000 ppm in the spectrum of NRs300, and to a lesser extent NRs700, may be assigned to the surface oxygen ions in hydrated (110) surfaces according to previous studies on ceria (100)[18] and (111)[30] surfaces, given that NRs300 is dominated by (110) and (100) surfaces, and also overlaps with the ~1012 ppm resonance arising from hydrous (100) surfaces.[18]

The structures of hydrated (111) and (100) surfaces have previously been revealed by combining DFT calculations and NMR,[18,30] however hydrated ceria (110) surfaces have not been analyzed; DFT simulations were therefore performed here. Quantitative ^1H NMR (Fig. S11, Table S4 and Note S1†) allows the concentration of hydrogen at the surfaces to be calculated (as surface hydroxyl groups and/or molecularly adsorbed water molecules), giving an estimated coverage of 1.5 water molecules

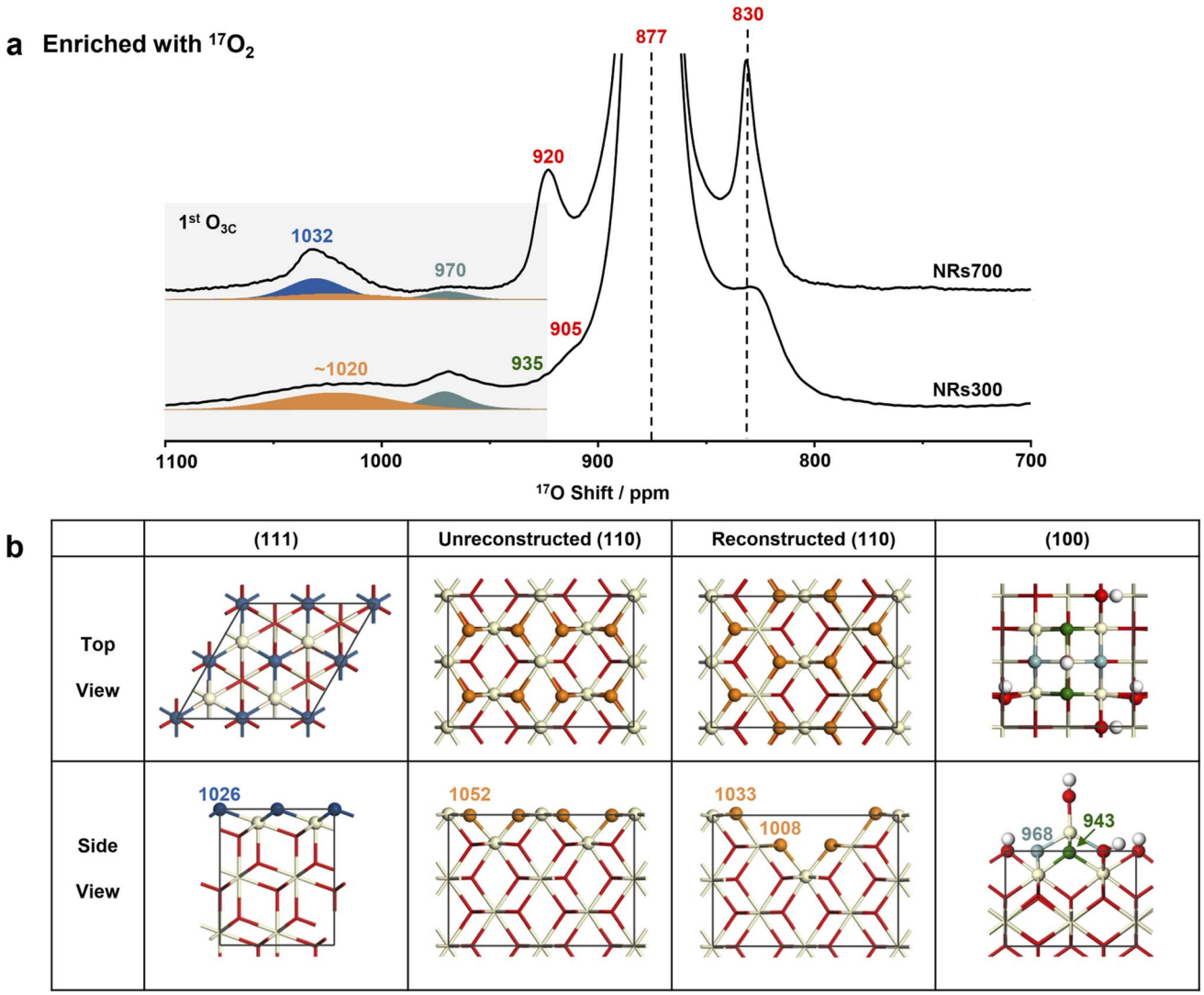

Fig. 2 ^{17}O NMR spectra (9.4 T), morphology diagrams and the dry structure model of ceria NRs700 and NRs300. (a) ^{17}O solid-state NMR spectra of the $^{17}O_2$-enriched ceria NRs700 and NRs300. The spectra were recorded at a spinning speed of 20 kHz and a 2.0 s recycle delay using a rotor synchronized Hahn-echo pulse sequence ($\pi/2-\tau-\pi-\tau$-acquisition) with ^{1}H decoupling. (b) The calculated structures of ceria (111), (110) and (100) surfaces. Red, off-white and white spheres denote bulk oxygen, hydrogen and cerium ions, respectively. 1st-layer oxygen ions from different surfaces are shown in different colors.

per surface unit for the (110) facets (83.9 Å^2, shown in Fig. 2b and Table S4†). We then performed DFT simulations of the ^{17}O shifts (δ_{CG}s) and adsorption energy (E_{ads}) with one water molecule per surface unit of hydrated ceria (110) surfaces.

Ten different models were considered: unreconstructed O-terminated models with dissociative and molecular water adsorption (UOD and UOM, respectively), four different reconstructed models with molecular adsorption (ROMa–ROMd), and four reconstructed models with dissociative adsorption (RODa–RODd). The water adsorption energies, E_{ads}, are summarized in Fig. S12.† On the basis of energetic favorability (more negative E_{ads}), models UOD, UOM, RODb and ROMb are the best representations of the structure of the hydrated (110) surface, therefore the ^{17}O shifts were calculated (Fig. S13–S24 and Tables S5–S8†). The broadness of the resonance at ~1000 ppm for $H_2{}^{17}O$ labeled NRs300 arises from the overlap of the different environments for O_{3C}s in ceria (110) surfaces represented in these models (Fig. 4, S25 and Tables S5–S8†), and further includes the shift at 996 ppm due to the 1st layer O_{3C}s in hydrated (100) surfaces.[18] The shoulder at 900 ppm in the experimental spectrum also arises from 1st layer O_{3C} ions in unreconstructed ceria (110) O-t surfaces with molecularly adsorbed water (UOM) (Fig. 4, S17, S18 and Table S6†). Fig. 3b summarizes the models for the (110) surface and the previously determined models for (111)[30] and (100)[18] hydrated surfaces. The calculated ^{17}O shifts (δ_{CG}s) of the 1st layer O_{3C}s in all these models are summarized in Fig. 4.

We now compare the surface structures of ceria low-index surfaces ((111), (110) and (100)) at dry and hydrated conditions (Fig. 4 and Table S9†). For all three facets, the molecular or dissociative adsorption of water results in distinctive changes to the ^{17}O shifts for oxygen species on the surface. The (111)

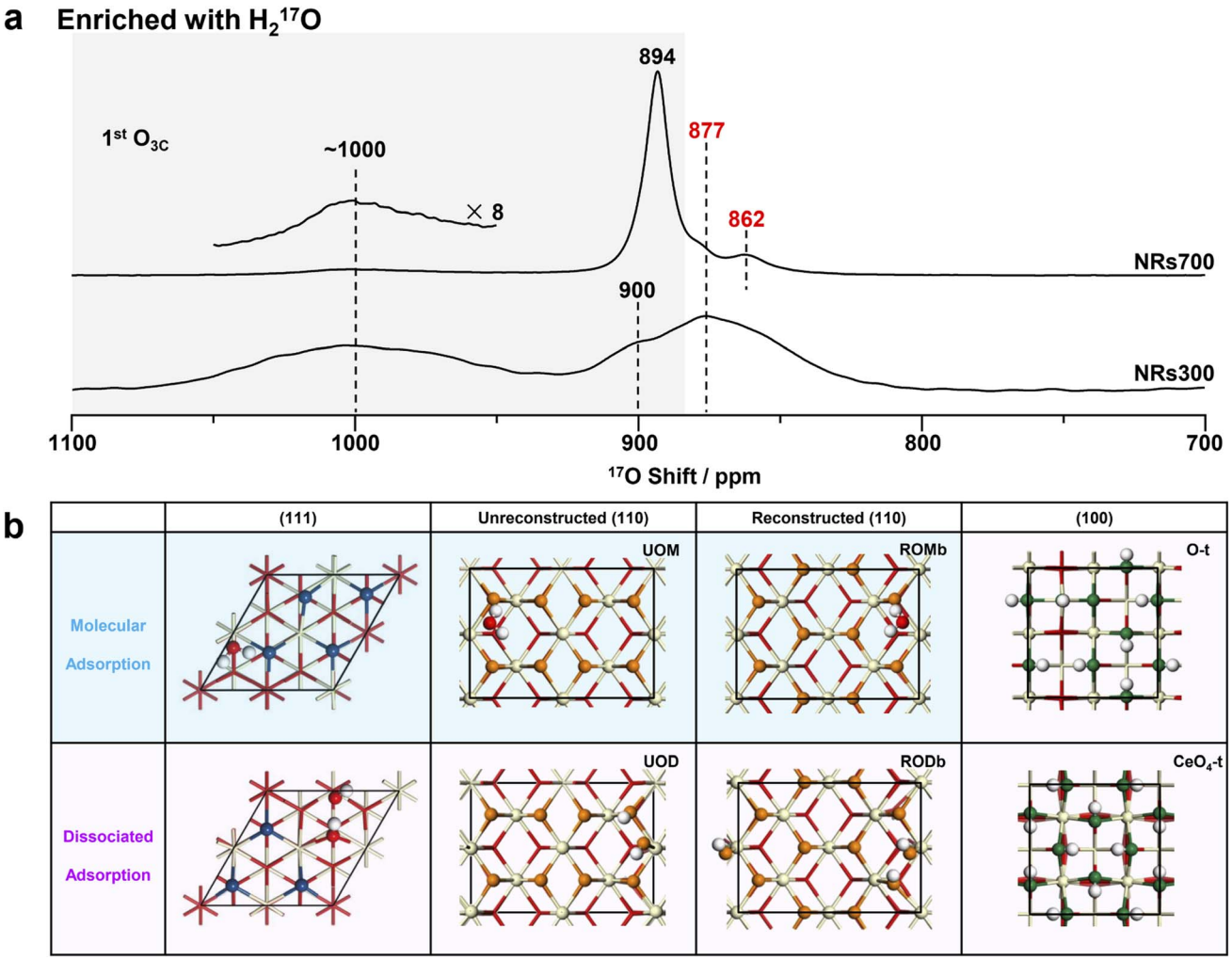

Fig. 3 ^{17}O NMR spectra of NRs700 and NRs300 and the hydrated structure models of ceria (111), (110) and (100) surfaces. (a) ^{17}O solid-state NMR spectra of the $H_2{}^{17}O$-enriched ceria NRs700 and NRs300 (with hydrated surfaces). The conditions under which these spectra were collected were consistent with the two in Fig. 2a. (b) The calculated structures of hydrated ceria (111), (110) and (100) surfaces. Red, off-white and white spheres denote bulk oxygen, hydrogen and cerium ions, respectively. 1st layer oxygen ions with variable chemical shifts are marked in different colors. O-t and CeO_4-t are O-terminated and CeO_4-t ceria (100) surfaces, respectively.[18]

surface comprises O_{3C}s in the 1st layer and O_{4C}s in the subsurface and bulk; the (110) surface is partially reconstructed into indent (111) nanofacets, with both reconstructed and unreconstructed surfaces comprising exposed O_{3C}s and inner O_{4C}s; the (100) surface consists of reconstructed oxygen-terminated (O-t) and CeO_4-terminated (CeO_4-t) surfaces.[18] Water molecules are adsorbed molecularly and dissociatively on the (111) and (110) surfaces, whereas only dissociative adsorption is observed for (100) surfaces, due to the presence of lower-coordinated oxygen ions.[18] The adsorbed water molecules in turn affect the coordinated 1st layer oxygen ions, *i.e.*, transform 1st layer O_{3C}s into surface hydroxyl groups by dissociation and coordinate with 1st layer O_{3C}s *via* hydrogen bonding on molecular adsorption; the ^{17}O shifts of these surface oxygen ions that are affected directly by the water molecule are shown on the left of Fig. 4. More interestingly, hydration also slightly perturbs the chemical environment of the adjacent O_{3C}s (all of the exposed 1st layer O_{3C}s shown in Fig. 3b) that are not directly bonded to water molecules, generating ^{17}O NMR shifts in between those of dry surfaces and the directly hydrated surface oxygens; these are shown on the right of Fig. 4. The observation that interactions between exogenously coordinated water and the surfaces can modify the chemical environment of both the immediately coordinated and surrounding ions suggests that not only the surface geometry but the impact of exogenous water should be carefully considered when investigating the "true" chemical environment of oxide surfaces.

CO adsorption on the pristine and hydrated (1/4 ML) ceria (111) surfaces were modeled and the adsorption energies were calculated to explore the effects of adsorbed H_2O (Fig. S26†). It is clear that a hydrous surface can lead to a slightly stronger CO adsorption on the bare oxygen sites, and the change might affect reactions involving CO with the presence of H_2O (Fig. S27 and Table S10†), which has been observed previously.[40,41] Comparing the three bare oxygen sites, the calculated CO adsorption energies suggest that the oxygen ions associated

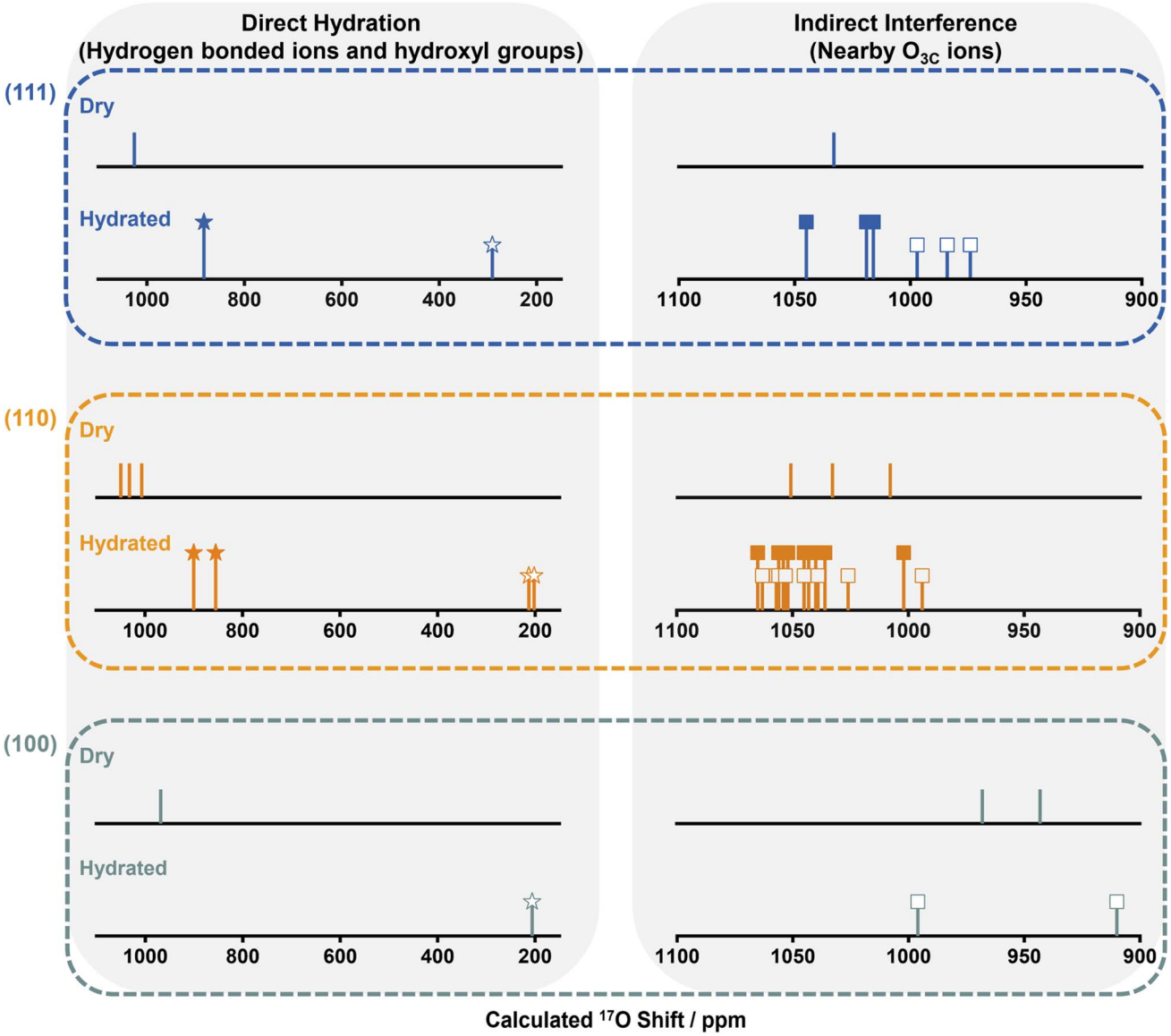

Fig. 4 Summarized ^{17}O NMR shifts (δ_{CG}s) predicted for the 1st layer oxygen ions in dry and hydrated ceria (111), (110) and (100) surfaces. At hydrous conditions, ^{17}O shifts of 1st layer oxygen ions interacting directly and indirectly with water molecules are denoted by stars and squares, respectively; while hollow and solid shapes represent the ^{17}O shifts of the 1st layer oxygen ions associated with dissociative and molecular water molecules, respectively.

with a smaller ^{17}O chemical shift are inclined to have stronger adsorption (Fig. S28 and Table S10†). Therefore, the ^{17}O NMR shift might be correlated to gas adsorption capability and thus the catalytic activity of a specific oxygen site.

Conclusions

The ceria (111), (110) and (100) facet structures, considering both geometry and the influence of external coordinated water molecules, were investigated with ^{17}O solid-state NMR in combination with DFT calculations. Tri-coordinated oxygen ions in the 1st layer of different dry ceria facets exhibit notable differences in their ^{17}O NMR shifts, resulting in a characteristic "spectral fingerprint" corresponding to the different surface geometries. The spectral signatures change under hydrous conditions, indicating that the chemical environment of the oxygen ions in hydrated oxide surfaces depends not only on the original surface geometry, but also on the interaction with adsorbed water molecules. Thus, the exogenously coordinated water is important and its interaction with the surface is a non-negligible factor when studying oxide surfaces, especially for oxide surfaces with complex structures (*e.g.*, ceria (110) and (100) surfaces exhibiting reconstructions) which may result in multiple adsorption sites and modes. The extension of this work to study the 'true' surface chemical environment and identify which oxygen species are involved under specific conditions (*e.g.*, temperature, pressure, and adsorption of guest species) can be envisaged. The insights obtained from this work

are expected to help to further the understanding of chemical processes at oxide surfaces.

Experimental section

Preparation of ceria NRs700 and NRs300

0.98 g $Ce(NO_3)_3 \cdot 6H_2O$ (Sigma-Aldrich, 99.9%) was dissolved in 20 mL distilled water. Then 15 mL NaOH (pH = 14) solution was quickly added and stirred for 30 minutes. The prepared solution was transferred to two 50 mL polytetrafluoroethylene hydrothermal reactors. After heating at 100 °C for one day, yellow precipitates were obtained. After washing with distilled water six times, the precipitates were dried at 80 °C overnight. The yellow powders were calcined at 700 and 300 °C for 5 hours, respectively. The two samples are denoted NRs700 (nanorods and calcined at 700 °C) and NRs300 (nanorods and calcined at 300 °C).

^{17}O isotopic labeling

150 mg sample was added into a glass tube and evacuated at 300 °C for 2 hours. After cooling down to room temperature, 90% ^{17}O-enriched O_2 gas/H_2O vapor was introduced into the tube and then heated at 300 °C for 48 hours for $^{17}O_2$ labeling and room temperature for 3 hours for $H_2{}^{17}O$ enrichment. The sample was re-evacuated and this process repeated (filling and evacuation) for four times to obtain highly ^{17}O labeled samples. After the final enrichment, the sample was re-evacuated at room temperature to remove residual $^{17}O_2$/$H_2{}^{17}O$.

^{17}O solid-state NMR spectroscopy

^{17}O magic angle spinning nuclear magnetic resonance (MAS NMR) spectra were measured on a 9.4 T Bruker Avance III 400 spectrometer, corresponding to a ^{17}O Larmor frequency of 54.2 MHz. Samples were packed into 4 mm outer diameter ZrO_2 rotors in a N_2-filled glove box. ^{17}O shifts were referenced to H_2O at 0.0 ppm.

^{17}O direct DNP NMR experiments were performed on a 14.1 T Bruker Avance III HD 600 spectrometer equipped with a 395 GHz gyrotron microwave source and a 3.2 mm MAS probe at a Larmor frequency of 81.3 MHz. Samples were mixed with radical solution (16 mM TEKPol[42] in dried tetrachloroethane, TCE) in an Ar-filled glove box. ^{17}O chemical shifts of the DNP NMR spectra were referenced to bulk ceria at 875 ppm at 100 K.

Data availability

Requests for materials and data can be addressed to Luming Peng.

Author contributions

J. Chen, X.-P. Wu, M. A. Hope, C. P. Grey and L. Peng conceived and developed the idea of the project. J. Chen and Z. Lin carried out the synthesis of ceria nanorods. J. Chen, L. Zhu, Y. Wen, Y. Zhang, T. Qin, T. Liu, X. Xia, D. Wu, and X. Liu carried out XRD, HRTEM, XPS, Raman, Na and N element analysis, and surface area measurement. J. Chen, Z. Lin, Y. Wen, and L. Peng performed ^{17}O isotope enrichment, collected and analysed the NMR spectra. J. Chen, M. A. Hope, and C. P. Grey collected and analysed the high field ^{17}O DNP NMR spectra; X.-P. Wu, J. Wang, and X.-Q. Gong conducted the DFT calculations. J. Chen, X.-P. Wu, M. A. Hope, W. Tang, W. Ding, X.-Q. Gong, L. Chen, and L. Peng wrote the manuscript and all authors discussed the experiments and final manuscript.

Conflicts of interest

There are no conflicts to declare.

Acknowledgements

This work was supported by National Key R&D Program of China (2021YFA1502803), the National Natural Science Foundation of China (NSFC) (21972066, 91745202, 21573103, 22003016 and 21421004), NSFC – Royal Society Joint Program (21661130149), the Fundamental Research Funds for the Central Universities (1124020512) and National Science Fund for Talent Training in Basic Science (J1103310). Junchao Chen would like to thank Dr Xingmin Zhang at Shanghai Institute of Applied Physics for his invaluable discussions and help in this work. The ECUST group thanks the Programme of Introducing Talents of Discipline to Universities (B16017). Luming Peng thanks the Royal Society and Newton Fund for a Royal Society – Newton Advanced Fellowship. Clare P. Grey thanks the European Research Council for an Advanced Fellowship. This work was also supported by the Research Funds for the Frontiers Science Center for Critical Earth Material Cycling, Nanjing University, and a project funded by the Priority Academic Program Development of Jiangsu Higher Education Institutions.

References

1 H. G. Yang, C. H. Sun, S. Z. Qiao, J. Zhou, G. Liu, S. C. Smith, H. M. Cheng and G. Q. Lu, *Nature*, 2008, **453**, 638–641.
2 W. Huang, *Acc. Chem. Res.*, 2016, **49**, 520–527.
3 X. Xie, Y. Li, Z.-Q. Liu, M. Haruta and W. Shen, *Nature*, 2009, **458**, 746–749.
4 Y. Li and W. Shen, *Chem. Soc. Rev.*, 2014, **43**, 1543–1574.
5 Z. Zhang, S.-S. Wang, R. Song, T. Cao, L. Luo, X. Chen, Y. Gao, J. Lu, W.-X. Li and W. Huang, *Nat. Commun.*, 2017, **8**, 488.
6 W.-C. Huang, L.-M. Lyu, Y.-C. Yang and M. H. Huang, *J. Am. Chem. Soc.*, 2012, **134**, 1261–1267.
7 T. Tachikawa, S. Yamashita and T. Majima, *J. Am. Chem. Soc.*, 2011, **133**, 7197–7204.
8 Y. Bi, S. Ouyang, N. Umezawa, J. Cao and J. Ye, *J. Am. Chem. Soc.*, 2011, **133**, 6490–6492.
9 H. Wang, K. Dou, W. Y. Teoh, Y. Zhan, T. F. Hung, F. Zhang, J. Xu, R. Zhang and A. L. Rogach, *Adv. Funct. Mater.*, 2013, **23**, 4847–4853.
10 F. Wang, X. Wang, Z. Chang, Y. Zhu, L. Fu, X. Liu and Y. Wu, *Nanoscale Horiz.*, 2016, **1**, 272–289.

11 B. Ren, Y. Wang and J. Z. Ou, *J. Mater. Chem. B*, 2020, **8**, 1108–1127.
12 M. Liu, L. Piao, L. Zhao, S. Ju, Z. Yan, T. He, C. Zhou and W. Wang, *Chem. Commun.*, 2010, **46**, 1664–1666.
13 X.-L. Cheng, J.-S. Jiang, D.-M. Jiang and Z. J. Zhao, *J. Phys. Chem. C*, 2014, **118**, 12588–12598.
14 P. L. Hansen, J. B. Wagner, S. Helveg, J. R. Rostrup-Nielsen, B. S. Clausen and H. Topsøe, *Science*, 2002, **295**, 2053–2055.
15 T. W. Hansen, J. B. Wagner, P. L. Hansen, S. Dahl, H. Topsøe and C. J. H. Jacobsen, *Science*, 2001, **294**, 1508–1510.
16 L. A. Kibler, A. Cuesta, M. Kleinert and D. M. Kolb, *J. Electroanal. Chem.*, 2000, **484**, 73–82.
17 F. Esch, S. Fabris, L. Zhou, T. Montini, C. Africh, P. Fornasiero, G. Comelli and R. Rosei, *Science*, 2005, **309**, 752–755.
18 J. Chen, X.-P. Wu, M. A. Hope, K. Qian, D. M. Halat, T. Liu, Y. Li, L. Shen, X. Ke, Y. Wen, J.-H. Du, P. C. M. M. Magusin, S. Paul, W. Ding, X.-Q. Gong, C. P. Grey and L. Peng, *Nat. Commun.*, 2019, **10**, 5420.
19 C. Yang, X. Yu, S. Heißler, A. Nefedov, S. Colussi, J. Llorca, A. Trovarelli, Y. Wang and C. Wöll, *Angew. Chem., Int. Ed.*, 2017, **56**, 375–379.
20 A. Vimont, F. Thibault-Starzyk and M. Daturi, *Chem. Soc. Rev.*, 2010, **39**, 4928–4950.
21 W. Zhang, Z. Lin, H. Li, F. Wang, Y. Wen, M. Xu, Y. Wang, X. Ke, X. Xia, J. Chen and L. Peng, *RSC Adv.*, 2021, **11**, 25004–25009.
22 Y. Hu, B. Guo, Y. Fu, Y. Ren, G. Tang, X. Chen, B. Yue and H. He, *Chem. Commun.*, 2015, **51**, 14219–14222.
23 Y.-K. Peng, L. Ye, J. Qu, L. Zhang, Y. Fu, I. F. Teixeira, I. J. McPherson, H. He and S. C. E. Tsang, *J. Am. Chem. Soc.*, 2016, **138**, 2225–2234.
24 M. A. Henderson, *Surf. Sci. Rep.*, 2002, **46**, 1–308.
25 G. E. Brown, V. E. Henrich, W. H. Casey, D. L. Clark, C. Eggleston, A. Felmy, D. W. Goodman, M. Grätzel, G. Maciel, M. I. McCarthy, K. H. Nealson, D. A. Sverjensky, M. F. Toney and J. M. Zachara, *Chem. Rev.*, 1999, **99**, 77–174.
26 R. Mu, Z.-J. Zhao, Z. Dohnálek and J. Gong, *Chem. Soc. Rev.*, 2017, **46**, 1785–1806.
27 A. Verdaguer, G. M. Sacha, H. Bluhm and M. Salmeron, *Chem. Rev.*, 2006, **106**, 1478–1510.
28 Y. Li, X.-P. Wu, N. Jiang, M. Lin, L. Shen, H. Sun, Y. Wang, M. Wang, X. Ke, Z. Yu, F. Gao, L. Dong, X. Guo, W. Hou, W. Ding, X.-Q. Gong, C. P. Grey and L. Peng, *Nat. Commun.*, 2017, **8**, 581.
29 M. Wang, X.-P. Wu, S. Zheng, L. Zhao, L. Li, L. Shen, Y. Gao, N. Xue, X. Guo, W. Huang, Z. Gan, F. Blanc, Z. Yu, X. Ke, W. Ding, X.-Q. Gong, C. P. Grey and L. Peng, *Sci. Adv.*, 2015, **1**, e1400133.
30 J. Chen, M. A. Hope, Z. Lin, M. Wang, T. Liu, D. M. Halat, Y. Wen, T. Chen, X. Ke, P. C. M. M. Magusin, W. Ding, X. Xia, X.-P. Wu, X.-Q. Gong, C. P. Grey and L. Peng, *J. Am. Chem. Soc.*, 2020, **142**, 11173–11182.
31 S. Carrettin, P. Concepción, A. Corma, J. M. L. Nieto and V. F. Puntes, *Angew. Chem., Int. Ed.*, 2004, **43**, 2538–2540.
32 J. Kašpar, P. Fornasiero and M. Graziani, *Catal. Today*, 1999, **50**, 285–298.
33 J. A. Rodriguez, S. Ma, P. Liu, J. Hrbek, J. Evans and M. Pérez, *Science*, 2007, **318**, 1757–1760.
34 Y. Gao, R. Li, S. Chen, L. Luo, T. Cao and W. Huang, *Phys. Chem. Chem. Phys.*, 2015, **17**, 31862–31871.
35 J. Zhang, X.-Q. Gong and G. Lu, *Surf. Sci.*, 2015, **632**, 164–173.
36 M. A. Hope, D. M. Halat, P. C. M. M. Magusin, S. Paul, L. Peng and C. P. Grey, *Chem. Commun.*, 2017, **53**, 2142–2145.
37 Q. Z. Ni, E. Daviso, T. V. Can, E. Markhasin, S. K. Jawla, T. M. Swager, R. J. Temkin, J. Herzfeld and R. G. Griffin, *Acc. Chem. Res.*, 2013, **46**, 1933–1941.
38 F. Blanc, L. Sperrin, D. A. Jefferson, S. Pawsey, M. Rosay and C. P. Grey, *J. Am. Chem. Soc.*, 2013, **135**, 2975–2978.
39 P. Berruyer, L. Emsley and A. Lesage, *eMagRes*, 2018, **7**, 93–104.
40 T. Yan, J. Gong, D. W. Flaherty and C. B. Mullins, *J. Phys. Chem. C*, 2011, **115**, 2057–2065.
41 J. T. Calla and R. J. Davis, *Ind. Eng. Chem. Res.*, 2005, **44**, 5403–5410.
42 A. Zagdoun, G. Casano, O. Ouari, M. Schwarzwälder, A. J. Rossini, F. Aussenac, M. Yulikov, G. Jeschke, C. Copéret, A. Lesage, P. Tordo and L. Emsley, *J. Am. Chem. Soc.*, 2013, **135**, 12790–12797.